Near-visible ultraviolet light induces a novel ubiquitous calcium-permeable cation current in mammalian cell lines

Francisco Mendez and Reinhold Penner

Max-Planck-Institute for Biophysical Chemistry, Am Fassberg, 37077 Göttingen, Germany

(Received 20 August 1997; accepted after revision 31 October 1997)

1. We studied the immediate and short-term effects of UV light in the near-visible range at the cellular and membrane level using the whole-cell patch-clamp technique in combination with digital fluorescence imaging.
2. Illumination with monochromatic UVA light (340–380 nm) induced a sustained non-saturable increase in membrane conductance dependent on wavelength and light intensity in several different mammalian cell types including RBL, mast, HEK, PC12 and 3T3 cells.
3. The current was non-selective for cations and permeable to Ca^{2+}, but was inhibited by trivalent cations and was not due to the activation of an endogenous ion channel. We termed this novel current I_{LiNC} for light-induced non-selective cation current.
4. A similar current was evoked by chemical peroxidants such as hydrogen peroxide and tert-butylhydroperoxide, but not by cytosolic oxidized glutathione.
5. The free-radical scavengers tocopherol (vitamin E) and ascorbic acid (vitamin C) significantly reduced the UV light effect.
6. The generation of the current was membrane delimited since it could be induced by the same UVA treatment in cell-free membrane patches showing a similar wavelength dependence.
7. These results suggest that I_{LiNC} is activated by UVA light-induced generation of free radicals acting through lipid or protein peroxidation, and may represent a ubiquitous mechanism by which Na^+ and Ca^{2+} can enter cells after phototoxic or free radical-induced membrane damage.

Excessive sunlight in the ultraviolet (UV) range is involved in pathophysiological events such as photoaging, inflammation, cancer, necrosis and apoptosis (Godar & Lucas, 1995). The phenomenology of UV irradiation has been characterized in some detail (Ziegler *et al.* 1994), usually focusing on the long-term effects on humans exposed to ambient sunlight (Gies, Roy, Toomey, MacLennan & Watson, 1995) or on the biochemical and pathological alterations observed after experimentally controlled UV exposure of cell populations (Vile, Basu-Modak, Waltner & Tyrrell, 1994).

From these studies it is evident that excessive UV light in the near-visible range acts in a similar way to ionizing radiation and oxidative stress, evoking numerous cellular responses that may range from mild to severe erythema to malignant transformation of dermal tissues. At the cellular level, the most important macroscopic effects observed after UV irradiation appear to be lipid peroxidation (Morliere, Moysan, Santus, Huppe, Maziere & Dubertret, 1991; Beer, Olvey, Miller, Thomas & Godar, 1993), increases in intracellular calcium concentration (Kimura, Maeda & Hayashi, 1992), loss of potassium (Cardenas, Cortes, Fernandez & Pena, 1992) and activation of protein kinases (Devary, Gottlieb, Smeal & Karin, 1992; Kasid, Suy, Dent, Ray, Whiteside & Sturgill, 1996; Verheij *et al.* 1996). The most severe consequences are cell swelling due to sodium influx (Koliwad, Kunze & Elliott, 1996*b*) and immediate apoptotic cell death (Beer *et al.* 1993; Godar & Lucas, 1995). However, little is known about the acute effects at the single-cell level and the underlying molecular mechanisms.

We have therefore carried out whole-cell patch-clamp recordings to investigate more immediate events due to UVA, the predominant UV species in our atmosphere. The main advantage of using this technique compared with cell biological and molecular approaches is the possibility for measuring UV effects in single cells rather than in populations. This allowed us to determine the dynamics and kinetics of membrane damage currently generalized under the broad and non-specific term 'phototoxic effects'. Our findings suggest that UV light in the near-visible range can activate a novel calcium-permeable cationic current. This current may be the basis for early cellular events following exposure to ionizing irradiation. Since UV light at relatively high intensity is used in a variety of experimental techniques applied to living cells (e.g. confocal microscopy, fluorescence

imaging techniques), these results not only yield important information regarding the pathophysiological alterations induced by UV light in general, but they are also relevant for the interpretation of data obtained from studies employing UV illumination.

METHODS

Cells

RBL-1 (rat basophilic leukaemia), 3T3 (mouse fibroblast), PC12 (phaeochromocytoma) and HEK (human embryonic kidney) cells were obtained from the American Tissue Type Culture Collection and cultured as previously described (Fasolato, Hoth & Penner, 1993*b*). RBL-2H3 cells were a kind gift from T. Jovin (MPI Biophysical Chemistry, Göttingen, Germany). Rat peritoneal mast cells were prepared according to Mathews *et al.* (1989).

Materials and solutions

Experiments were usually performed in standard saline containing (mM): NaCl, 140; KCl, 2·8; CsCl, 10; $CaCl_2$, 1; $MgCl_2$, 2; glucose, 11; Hepes-NaOH, 10. The pH was adjusted with NaOH to 7·2. Patch-clamp pipettes were filled with the standard intracellular solution containing (mM): caesium glutamate, 145; NaCl, 8; $MgCl_2$, 1; Mg-ATP, 2; Mg-GTP, 0·3; K_2-EGTA, 6·6; Ca-EGTA, 3·3 resulting in a free calcium concentration of ~80 nM, pH 7·2 (adjusted with CsOH). In order to measure inwardly rectifying potassium currents in some experiments, extracellular CsCl was omitted and the external KCl concentration was increased to 20 mM instead. Under these conditions, intracellular caesium glutamate was replaced by potassium glutamate (pH adjusted with KOH). Solution osmolarity was between 295 and 310 mosmol l^{-1} for internal and external solutions.

To study the influence of antioxidants, either 10 mM sodium ascorbate was added to the internal solution or the cells were incubated for 2 h at 37 °C in a medium supplemented by 10 i.u. (+)-α-tocopherol. Fast extracellular solution changes were made by local application with a wide-tipped micropipette from a distance of about 50 μm. Hydrogen peroxide (H_2O_2; 60%) and tert-butyl-hydroperoxide (tBOOH; 70%) were diluted from stock into extracellular medium to a final concentration of 3 or 3·5% on the day of usage. If not stated otherwise, all chemicals were purchased from Sigma.

Electrophysiology

All patch-clamp experiments were performed using the tight-seal whole-cell configuration at room temperature (21–27 °C). Patch pipettes were pulled from Kimax glass, coated with Sylgard and fire polished. Their capacitance was below 6 pF and their resistance was between 1·5 and 2·5 MΩ after filling with the standard internal electrolyte. Access resistance during experiments was in the range 2–8 MΩ. High-resolution membrane currents were acquired by a computer-based patch-clamp amplifier system (EPC-9/Pulse; HEKA, Lambrecht, Germany). The currents were filtered at 2·9 kHz and sampled at a rate of 10 kHz. Capacitative currents were determined and compensated before each voltage pulse using the built-in automatic capacitance compensation of the EPC-9. Unless indicated otherwise, a standard pulse protocol consisting of a voltage ramp ranging from −100 to +100 mV (50 ms duration) followed by a constant voltage pulse to −40 mV (200 ms duration) was applied every 2 s from a holding potential of 0 mV (inset in Fig. 1*B*). Inward current and variance values shown in the figures correspond to the mean values of the second half of the constant pulse segment (100 ms duration or 1000 samples). Sometimes, the standard deviation of the current is shown instead of its variance which is the square root of the variance.

Calcium measurements

Free cytoplasmic calcium was measured by including 200 μM of the fluorescent calcium indicator dye fura-2 (pentapotassium salt; Molecular Probes) in the internal solution without further addition of EGTA or Ca-EGTA. The dye was excited alternately at 360 and 380 nm and free calcium was calculated from the fluorescence ratio F_{360}/F_{380} at 510 nm (Grynkiewicz, Poenie & Tsien, 1985). The calibration constants K_{eff} (effective K_D), R_{min} (fluorescence ratio in zero Ca^{2+}) and R_{max} (fluorescence ratio in saturating Ca^{2+}) were obtained from *in vivo* calibration experiments. Typical values were $R_{\text{min}} = 0{\cdot}95$, $R_{\text{max}} = 6{\cdot}2$ and $K_{\text{eff}} = 2{\cdot}4$ μM. Transmission and fluorescence images were digitally acquired using a Peltier-cooled slow-scan CCD camera with a 12-bit A/D converter and a resolution of 388 × 286 pixels (THETA SYSTEM, Gröbenzell, Germany). Fluorescence values from spatial regions of interest covering the cell somata were averaged off-line after subtracting the corresponding background fluorescence prior to the configuration of the whole-cell recording configuration.

UV irradiation

UV light was applied with a conventional commercial imaging system consisting of a monochromator equipped with a 75 W xenon lamp (T.I.L.L. Photonics, Munich, Germany), an inverse microscope (Axiovert 100; Zeiss), a ×40 oil-immersion objective lens (Fluar, Zeiss; numerical aperture of 1·3) and a beam splitter reflecting UV light below 410 nm towards the cell under observation. The monochromator allowed the adjustment of any discrete wavelength (± 2 nm) in the range 260–670 nm within 3 ms using a galvanometric scanner. The excitation light was directed from the monochromator to the microscope through a glass fibre cable. In most cases, the full intensity of the UV light (13–16 kW m^{-2}; cf. Fig. 2*C*) was used to irradiate the cells. In some experiments, light intensity was reduced by using quartz glass grey filters in the illumination pathway between the output of the glass fibre and the microscope. These filters had optical densities of 0·3 and 0·7, which resulted in 50 and 25% of the full light intensity, respectively. The intensity of the light beam was measured using a photodiode. All of the light was projected towards a circular spot of 240 μm diameter at the focus level. Cells were usually located in the centre of this spot resulting in a light intensity 15% higher than the mean value over the whole area (i.e. 14·9–18·5 kW m^{-2}).

Estimation of activation kinetics

In order to quantify the rate of activation of the inward current we fitted its time dependence to the following equation modified after the common description of voltage-activated ion channels according to Boltzmann replacing V (voltage) by t (time):

$$I(t) = \frac{I_{\text{max}} - I_0}{1 + \exp(-(t - t_0 - t_{½})/\text{slope})}, \quad (1)$$

where I_{max} (maximal current), $t_{½}$ (half the time to reach I_{max}) and slope are the free parameters to be fitted, I_0 corresponds to the inward current at the beginning of the illumination (t_0) and $I(t)$ to the inward current at time t. This formalism usually resulted in an accurate and reproducible estimation of the activation kinetics. Since the current we measured never saturated (cf. Fig. 6*A*), I_{max} – and therefore $t_{½}$ – are less reliable. We therefore chose to show only the resulting slope values (in s), with smaller values being equivalent to a faster activation.

RESULTS

To assess the effects of ultraviolet light on membranes of single cells, we carried out standard whole-cell recordings in rat basophilic leukaemia cells (RBL). Typically, about 3 min after establishing the whole-cell patch-clamp configuration, we illuminated the cell under investigation with ultraviolet light of the desired wavelength by using the monochromator of a conventional imaging system. Whole-cell break-in alone resulted in no changes of the overall electrical parameters like membrane potential or whole-cell conductance. The nominal light intensity for standard experiments was 18·5 kW m^{-2} at 380 nm and decreased due to the filter characteristics of the microscope to 14·9 kW m^{-2} at 340 nm (cf. Fig. 2*C*), which produces an equivalent of 1 MED (minimal erythema dose) in about 13 s (Lavker, Veres, Irwin & Kaidbey, 1995). This intensity applied for 30 s is comparable to UVA doses generated by 10–45 h of sunlight exposure (based on estimates of about 10 kJ h^{-1} m^{-2} prevailing on a typical midsummer day) and usually yielded a significant activation of the current described in the following. The membrane potential of the cell was clamped to 0 mV during the whole experiment. Every 2 s a voltage protocol was applied which consisted of a short 50 ms ramp from −100 to +100 mV followed by a constant 200 ms segment at −40 mV (cf. inset in Fig. 1*B*). The voltage ramp yielded the cell's current–voltage (*I*–*V*) relationship, which was used to determine the reversal potential (V_{rev}) and whole-cell resistance (R_m), while the last 100 ms of the

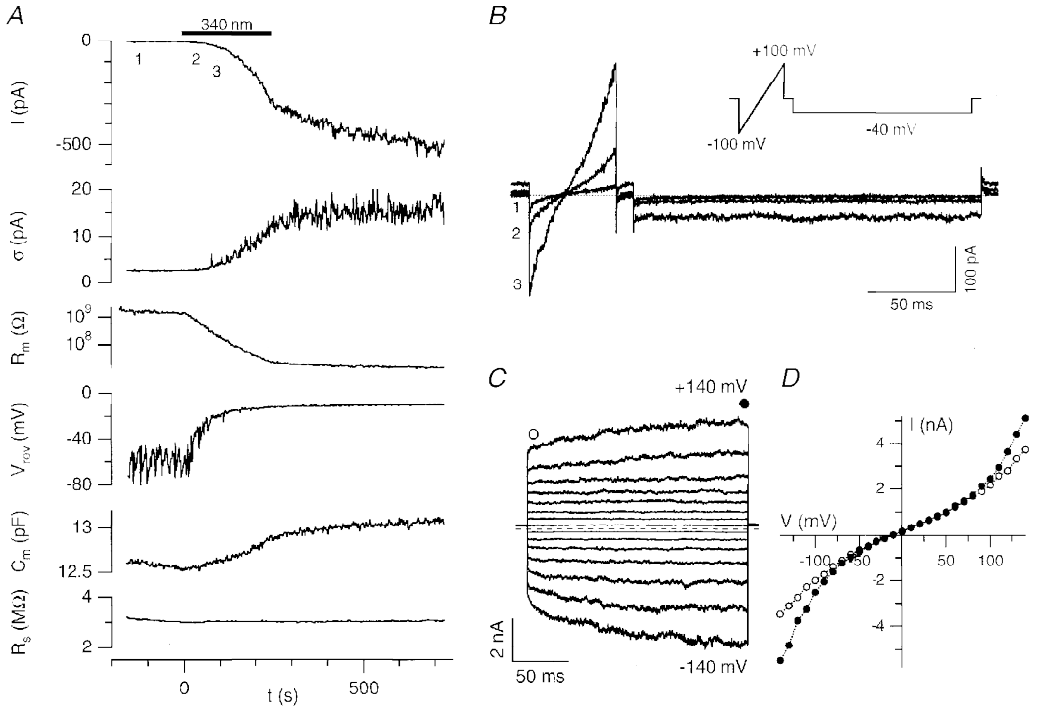

Figure 1. Typical example of whole-cell currents activated by UVA irradiation

All data shown were taken from a single RBL-1 cell representative of a total of more than 600 similar experiments. *A*, time dependence of activation of an inward current (*I*, upper trace) and its associated standard deviation (σ, second trace) recorded at −40 mV. At the time indicated by the bar, the cell was irradiated with UV light at 340 nm wavelength (4 min duration). Labels 1–3 indicate the time at which high-resolution voltage ramps were taken for display in panel *B*. Additional traces show the membrane resistance (R_m) and zero-current voltage (V_{rev}) of the cell as determined by linear regression of current records evoked by voltage ramps. Membrane capacitance (C_m) and series resistance (R_s) are displayed in the bottom two traces and were calculated every 2 s prior to the execution of the voltage pulse protocol shown in *B*. *B*, whole-cell current–voltage (*I*–*V*) relationship and inward current determined by voltage ramps and pulses before illumination (1), after 30 s (2) and 60 s (3) of illumination at 340 nm, respectively (see corresponding labels in *A*). Irradiation induced depolarization of the reversal potential, an increase in whole-cell conductance and a sustained inward current at −40 mV. The inset shows the pulse protocol that was executed repetitively every 2 s from a holding potential of 0 mV. *C*, whole-cell currents in response to hyper- and depolarizing voltage pulses in the range −140 to +140 mV from a holding potential of 0 mV at the end of the experiment. Note the voltage-dependent activation of the current below −60 and above +80 mV. Open (○) and filled (●) symbols indicate the times at which current amplitudes were determined to yield the *I*–*V* relationship shown in *D*. Current amplitudes were averaged over the first and last 5 ms periods of the current records shown in *C*.

constant segment were used to calculate the mean current (I) and its variance (σ^2) as shown in the upper two traces of Fig. 1*A*.

Ultraviolet light activates a novel cationic current (I_{LiNC})

Shortly after the onset of UV illumination, a sustained inward current (at −40 mV) developed (upper trace, Fig. 1*A*). As will be shown below, this is a novel non-selective cation current, and for simplicity, we will subsequently refer to this conductance as I_{LiNC} (for light-induced non-selective cation current). With sustained illumination, the membrane resistance continued to decrease (third trace, Fig. 1*A*), eventually approaching the range of the open patch pipette (< 20 MΩ) and making a further analysis impossible (cf. Fig. 6*A*). Therefore, in most experiments, illumination was discontinued as soon as the current amplitude reached about −150 to −300 pA (at −40 mV). Turning the UVA off usually abrogated a further activation and caused the current to stay at the actual level or to just slightly increase with time. The time course of activation of the conductance during illumination could not be fitted by a simple exponential or power-law equation. Nevertheless, to somehow assess the kinetic parameters of current activation, we used a modified Boltzmann equation, which yielded a semi-quantitative description of the kinetics during the irradiation phase, providing three parameters: (i) slope of activation, (ii) maximal current, and (iii) the time to reach half-maximal amplitude (see Methods). Obviously, since the current did not saturate, the fitted maximum current is the least accurate parameter. Thus, we consider the slope of activation a more meaningful parameter (summarized in Fig. 7*D*).

The inward current activated by UV light was paralleled by a characteristic increase in the current variance (second trace, Fig. 1*A*). A simple variance analysis of the current (after steady state was reached) yielded a unitary current i of −0·44 pA when fitted to the equation $\sigma^2 = iI - I^2/n$, where σ^2 is the variance, I is the whole-cell current and n is the number of ion channels. With the measured reversal potential of −12 mV, this corresponds to a unitary 'single channel' conductance g of 16 pS. Mean values pooled from twenty-three to twenty-five independent experiments under the same conditions were $g = 14 \pm 0{\cdot}8$ pS and $V_{rev} = -12 \pm 0{\cdot}35$ mV.

Voltage dependence of I_{LiNC}

The *I–V* relationship of the conductance was determined every 2 s by a voltage ramp (Fig. 1*B*). The control *I–V* relationship before illuminating at a wavelength of 340 nm showed no significant currents apart from a small linear leak (trace 1, Fig. 1*B*). After 30 s of illumination the *I–V* relationship became steeper, indicating an increase in whole-cell membrane conductance (trace 2, Fig. 1*B*). Another 30 s of illumination increased the current further (trace 3, Fig. 1*B*) without affecting its overall characteristics. The measured reversal potential was about −12 mV, which is slightly more negative than expected for a symmetric cationic current (as will be shown later, this deviation is probably due to a slight preference for K^+ and Cs^+ over Na^+ ions). Since the current was not linear but showed rectification at far positive and negative potentials (Fig. 1*B*; see also Fig. 1*C*), it was not caused by a simple breakdown of the seal resistance, but was due to a genuine ionic conductance. This is further supported by the fact that we were able to routinely obtain tight outside-out patches after activating the current (data not shown), indicating that the gigaseal between the patch pipette and the cellular membrane was still intact. Moreover, neither the series resistance nor the membrane capacitance, both calculated before each single sweep, changed significantly enough to indicate an unstable recording configuration induced by the irradiation. However, we usually observed a small increase in membrane capacitance during irradiation. It was on average 2·4 ± 0·17 % in 4 min ($n = 8$, mean value ± S.E.M.) and is presumably due to a change in the dielectrical constant of the membrane induced by peroxidation of the membrane lipids (as will be shown later).

To assess the voltage-dependent rectification at very positive and negative potentials, as well as possible time-dependent gating processes, we applied rectangular 200 ms pulses covering the voltage range between −150 and +150 mV (Fig. 1*C*). This protocol revealed that the conductance indeed exhibits both voltage and time dependence. When analysing the first 5 ms of the current responses, there was a rectification with a similar voltage dependence as seen in the voltage ramps (cf. ○ in Fig. 1*D* and trace 3 in Fig. 1*B*). In addition, at larger potentials (above or below ± 50 mV, respectively) the current further activated with time, reaching its maximum after 150 ms and thus generated even stronger rectification (● in Fig. 1*D*). In this voltage range the current's variance also increased in a non-linear way.

Wavelength and intensity dependence of I_{LiNC}

To determine whether this conductance was in fact activated by UV light, we studied the dependence of its activation on wavelength and intensity of irradiation by changing these parameters in a systematic fashion. The strongest activation was obtained at 340 nm (Fig. 2*A*). With longer wavelengths, the ability to activate the conductance decreased (although the power of the UV light increased by 24 % when going from 340 to 380 nm; Fig. 2*C*) and showed no effect at 400 nm (data not shown). Untreated cells were stable for up to 1 h in the whole-cell configuration without showing any increase in leak conductance (data not shown, but see Fig. 8*A*, which gives pooled data from cells irradiated after 15 min under whole-cell patch-clamp conditions). The activation slopes from fits according to eqn (1) (means ± S.E.M.) were 53 ± 5·5 s ($n = 10$) at 340 nm, 95 ± 10·5 s ($n = 12$) at 360 nm, and 162 ± 13·9 s ($n = 9$) at 380 nm (Fig. 7*D*). Due to instrument limitations we were not able to deliver sufficient light below 340 nm (Fig. 2*C*).

The intensity dependence of the UV-induced current was assessed at the most effective wavelength, i.e. 340 nm (Fig. 2*B*). Decreasing light intensity by a factor of 2 resulted in a doubling of illumination period required to activate the same magnitude of current. The current amplitudes (means ± S.E.M.) determined after 100 s at full light intensity, after 200 s at half the intensity, and after 400 s at one-quarter light intensity were quite similar: $-3{\cdot}9 \pm 1{\cdot}6$ pA pF^{-1} ($n = 6$), $-4{\cdot}3 \pm 1{\cdot}4$ pA pF^{-1} ($n = 4$) and $-4{\cdot}8 \pm 1{\cdot}2$ pA pF^{-1} ($n = 5$), respectively.

As for most experiments in this study, the above experiments were performed under standard conditions where cytoplasmic calcium was buffered to a low resting value of about 80 nM using a mixture of 6·6 mM EGTA and 3·3 mM Ca^{2+}-saturated EGTA. Varying the cytoplasmic free calcium concentration in the range between 80 and 320 nM by different mixtures of Ca-EGTA and EGTA (total EGTA concentration of 9 mM) resulted in no significant difference in light-induced activation of the current (slope = 45 ± 8·0, 66 ± 4·6 and 42 ± 3·5 s ($n = 6$) for 80, 160 and 320 nM, respectively; data not shown). Even buffering cytoplasmic calcium to zero by adding 9 mM EGTA (no Ca-EGTA) resulted in the same light-induced activation compared with control conditions (slope = 74 ± 11·0 s ($n = 7$); data not shown). However, under essentially unbuffered conditions (i.e. no additional buffers except 100 μM fura-2 or EGTA), the activation of the current was accelerated by a factor of 1·6 compared with the standard situation (slope = 32 ± 2·9 s ($n = 11$); data not shown). Thus, EGTA appears to attenuate the activation of the cation current. A similar protective action of calcium chelators has also been noticed in rabbit proximal tubule cells, where EGTA reduced lipid peroxidation and cell death (Schnellmann, 1991).

Selectivity of I_{LiNC}

From its reversal potential and fairly linear *I–V* relationship we conclude that the current is non-selective and permeable to cations. To test this in more detail, extracellular cations were exchanged by fast local superfusion. Replacing the

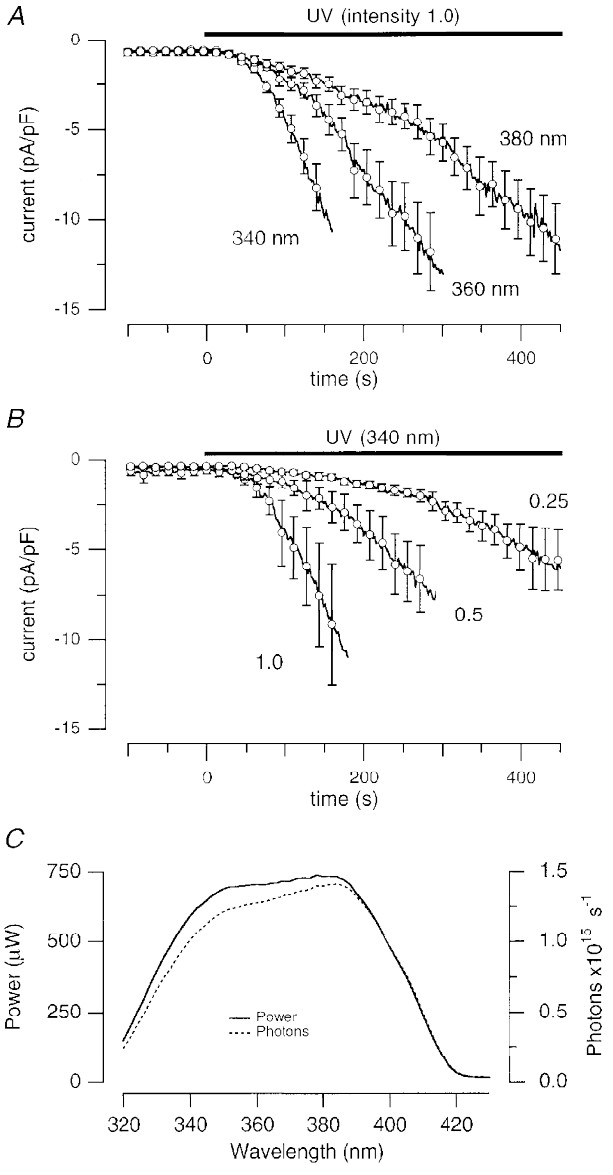

Figure 2. Activation of I_{LiNC} depends on wavelength and intensity of ultraviolet light

A, wavelength dependence of the UV-induced current was studied under equivalent light intensities by irradiating cells at 340, 360 and 380 nm. Due to the filter characteristics of the optics, the light intensity decreased with wavelength within the range shown (see panel *C*). The decrease was 20% when going from 380 to 340 nm. Nevertheless, activation of the current was more pronounced. Mean values ± S.E.M. of 9–12 independent experiments per wavelength are shown. *B*, intensity dependence was studied at the wavelength yielding maximal activation (340 nm) by decreasing the light intensity to one-half and one-quarter of the full unfiltered intensity with quartz grey filters (optical densities of 0·3 and 0·7) in the excitation pathway. Mean values ± S.E.M. of 4–6 cells per intensity are shown. *C*, UV light intensity and corresponding number of photons at different wavelengths. The UV light was projected by a glass fibre into a circular area with a diameter of 240 μm. The light intensity in the centre of this circle was 15% higher than the overall intensity.

standard Na^+-containing saline by solutions in which Cs^+ or K^+ were the main cations, revealed that both ions were slightly more permeant than Na^+, increasing the inward current by approximately 10% (see Fig. 3*A*). At the same time there was a slight shift in reversal potential. However, when extracellular Na^+ was replaced by larger cations like NMG^+ (Fig. 3*B*) or TEA^+, the inward current was greatly reduced without affecting the outward current, showing almost no influx at −40 mV. This suggests that NMG^+ is not a permeant ion, but at the same time fails to impede current flow in the outward direction. On the other hand, extracellular application of trivalent cations like La^{3+} or Gd^{3+} (Fig. 3*C*) potently inhibited both inward and outward currents (IC_{50} for Gd^{3+} was 23 μM ($n = 21$), Fig. 3*D*). Cd^{2+} was at least one order of magnitude less effective than trivalent cations in blocking the current (Fig. 3*D*).

It has been previously reported that UV light may cause a Ca^{2+} rise and immediate apoptosis in many cells and that these effects strongly depend on the wavelength (Godar & Lucas, 1995). We therefore tested for a possible Ca^{2+} permeability of this conductance. The experiment illustrated in Fig. 4*A* demonstrates that the UV light-induced conductance indeed leads to an enhanced Ca^{2+} influx into the cell. In this example, which is representative of twelve similar experiments, the cell was kept in the whole-cell configuration and fura-2 was allowed to diffuse into the cell from the patch pipette (seen as the exponential increase in fluorescence following the break-in). Intracellular Ca^{2+} concentration was assessed sparingly by brief ratiometric determinations at intervals of 20 s. After reaching steady-state conditions, the cell was exposed to more intense illumination (alternating cycles of 360 and 380 nm UV light at a rate of 1 Hz and 200 ms duration at each wavelength), which resulted in the activation of an inward current. At the same time, the membrane potential of the cell was alternately clamped to 0 and −60 mV, where the negative potential was designed to increase the driving force for Ca^{2+} into the cell. While the same voltage excursions were ineffective at changing $[Ca^{2+}]_i$ prior to the activation of the conductance, they did so after activation (Fig. 4*A*). Thus, each hyperpolarization induced a steeper increase in $[Ca^{2+}]_i$ after UV light exposure had triggered the cationic conductance. The cytoplasmic free calcium concentration

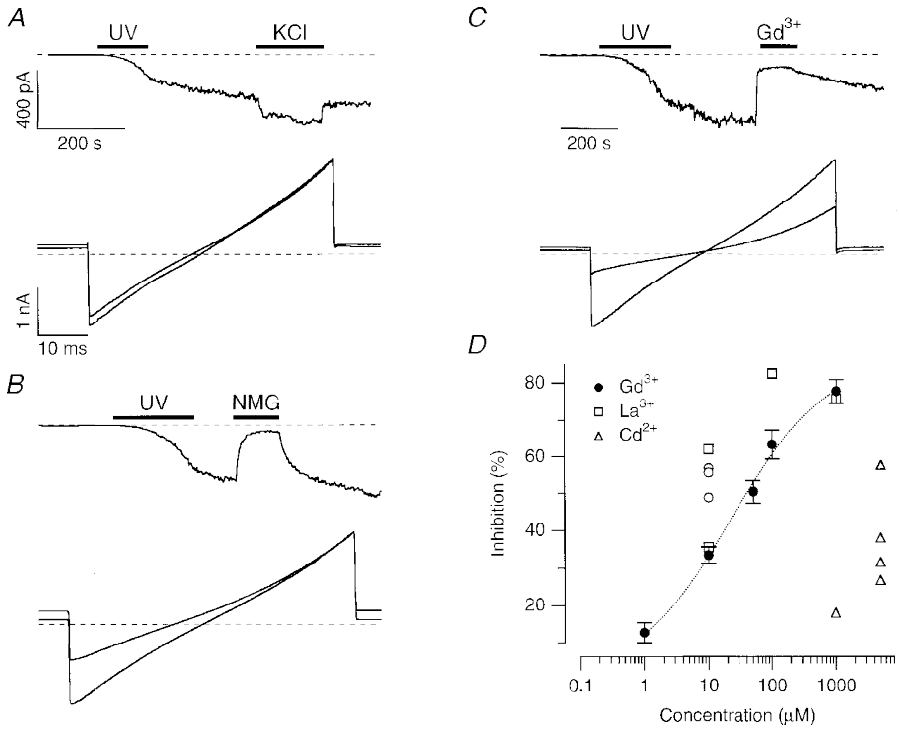

Figure 3. Selectivity of I_{LiNC} and its inhibition by trivalent cations

A, the upper trace shows the inward current at −40 mV. At the time indicated by the first bar, the cell was irradiated with UV (340 nm). After activation of I_{LiNC}, the cell was superfused temporarily by a local application, indicated by the second bar, of an external solution in which NaCl was replaced by 150 mM KCl. The lower traces are averages of 20 voltage ramps from −100 to +100 mV before and during exchange of the extracellular bath medium. *B*, same as *A*, except that the application solution contained 150 mM NMGCl. *C*, same as *A*, except that 100 μM $GdCl_3$ was added to the standard extracellular solution. *D*, dose–response curve showing the inhibition of I_{LiNC} at −40 mV in RBL-1 cells by Gd^{3+} (●, the dotted line represents a fit yielding an IC_{50} of 23 μM), La^{3+} (□) and Cd^{2+} (△), and in PC12 cells by Gd^{3+} (○). Each open symbol corresponds to the inhibition measured in a single cell, whereas the filled symbols are means ± S.E.M. of at least 4 independent determinations.

did not further increase significantly after returning to a holding potential of 0 mV, while the inward current increased slightly after switching the frequency of UV excitation back to 0·05 Hz.

Further support for the UV light-induced current being calcium permeable came from experiments in which the extracellular solution was replaced by isotonic Ca^{2+} solution (75 mM $CaCl_2$). Under these conditions, inward current amplitudes were reduced but were still as much as 50% of those of control cells (Fig. 4*B* and *C*), while outward currents were hardly affected (Fig. 4*C*). Together, these data suggest that Ca^{2+} acts as a permeant blocker. These characteristics are similar to those of other non-selective cation currents (Fasolato, Hoth, Matthews & Penner, 1993*a*).

I_{LiNC} is a ubiquitous membrane conductance

In order to identify the molecular mechanism involved in the activation of I_{LiNC} we tested the effects of UVA on cell-free membrane patches, by studying outside-out patches excised from RBL cells and using the same conditions and voltage protocols as for the whole-cell patch-clamp recordings presented in Fig. 1. Following irradiation with UVA, the membrane conductance in these patches invariably increased and yielded a sustained inward current ($n = 12$). The current activation showed kinetics and wavelength dependence quite similar to the whole-cell conductance (Fig. 5*A*). In addition, we detected 'single channel'-like current fluctuations at early stages of UVA irradiation (Fig. 5*B*). These fluctuations had a linear *I–V* relationship with a voltage dependence that was similar to the whole-cell currents. At higher voltages, there was an increase in the 'open probability', which could account for the macroscopic characteristics described earlier (i.e. voltage-dependent activation and increase in current noise). It thus appears that the UVA-induced conductance is membrane delimited and unlikely to require cytosolic factors.

To characterize further the time dependence of I_{LiNC}, additional experiments were carried out with different illumination delays, durations and intervals. Prolonged continuous illumination caused the membrane resistance to continuously decrease with time, ending up at values of less than 20 MΩ and thus making further patch-clamp experiments impossible (Fig. 6*A*). Thus I_{LiNC} appears to be unsaturable. In addition, the current, once activated by UV light or peroxidant treatment (see below), did not inactivate or run down, even over a time period of more than 30 min after the triggering event (Fig. 6*A*). Multiple UVA exposure with intermittent pauses revealed that the activation of the current is cumulative (Fig. 6*B*). Hence, the activation of I_{LiNC} is equivalent when either the same amount of UV light

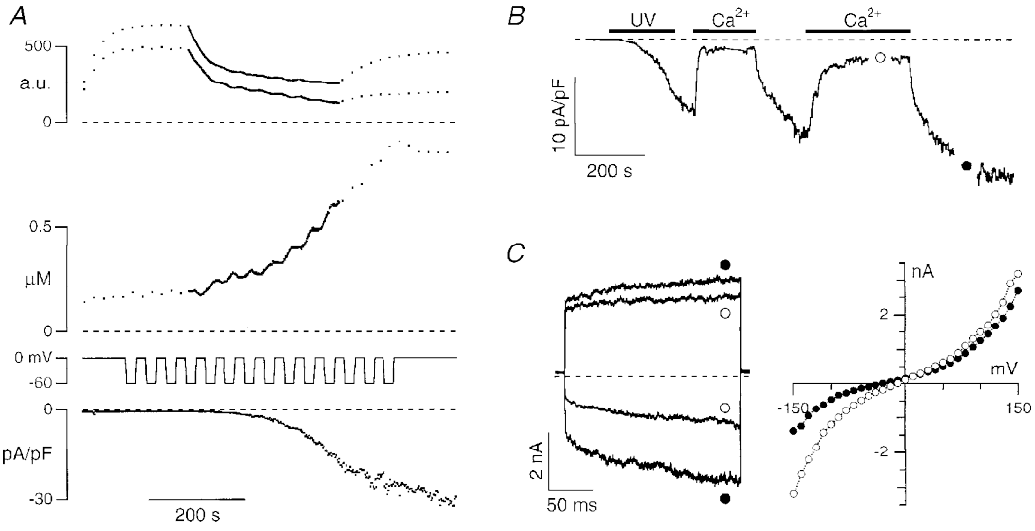

Figure 4. Ultraviolet light induces calcium influx

A, a single cell was investigated using combined patch-clamp and calcium-imaging techniques. After establishing the whole-cell recording configuration, loading of the calcium indicator dye fura-2 (200 μM) was monitored by dual-wavelength excitation (360 and 380 nm) at a frequency of 0·05 Hz and irradiation of 200 ms per wavelength (upper trace). When equilibrium was reached, excitation frequency was switched to 1 Hz. This caused significant bleaching of the fluorescent dye (upper trace; a.u., arbitrary units), an increase in cytoplasmic free calcium concentration (second trace), and a sustained inward current at a potential of −40 mV (lower trace). The pipette holding potential was alternately hyperpolarized every 20 s from 0 to −60 mV in order to increase the driving force for calcium influx. *B*, calcium permeability of the UV-induced current. The experimental conditions were the same as in Fig. 3*A–C*. The last two bars indicate replacement of the external standard solution by 75 mM $CaCl_2$ (10 mM Hepes, pH 7·2). At the time depicted by the circles a voltage pulse protocol was given as shown in Fig. 1*C*. *C*, the left panel shows whole-cell currents at −140 mV and +140 mV in normal (●) and isotonic Ca^{2+} (○) external solution. The right panel shows the complete *I–V* relationship.

is applied as a single continuous illumination period or split up into several shorter illuminations, provided the light intensities and the total durations are identical. The current magnitude and the kinetics of activation were the same in both cases.

The UVA-induced current with the above characteristics was not restricted to RBL cells, but could also be evoked in several other cell types, including 3T3 fibroblasts ($n = 5$), HEK cells ($n = 6$), PC12 cells ($n = 11$) and mast cells ($n = 5$). Figure 6*C* gives some representative examples of UV light-induced currents in these cells.

Chemical peroxidants induce a LiNC-like current

UVA is known to cause peroxidation by a radical chain reaction (Bose, Agarwal & Chatterjee, 1990; Stark, 1991). If the cation current was activated by a peroxidation process, a similar current should also be induced as a consequence of oxygen radical stress due to chemical peroxidants, and free radical scavengers should be effective in inhibiting the activation of the current. Therefore, free radical scavengers such as ascorbic acid and tocopherol were tested for possible antagonistic actions on the activation of the light-activated current. As shown in Fig. 7*A* and summarized in Fig. 7*D*, both vitamins C and E slowed the activation kinetics of the cationic current considerably. Perfusing cells with pipette solutions containing 10 mM sodium ascorbate (vitamin C) reduced the slope of activation from $60 \pm 8{\cdot}4$ s ($n = 5$) to $80 \pm 6{\cdot}7$ s ($n = 8$). Preincubation of cells for 2 h with 10 i.u. (+)-α-tocopherol (vitamin E) was even more effective in antagonizing the activation of the conductance, yielding a slope of $98 \pm 5{\cdot}1$ s ($n = 8$) at 340 nm. This activation rate is equivalent to a 50% reduction in light intensity or shift in wavelength from 340 to 360 nm (Fig. 7*D*).

Further evidence for the involvement of a peroxidation mechanism in the activation of the UVA current was obtained when applying chemical peroxidants, which activated a very similar current (Fig. 7*B*). In whole-cell recordings, 3% H_2O_2 ($n = 15$) or 3·5% tBOOH ($n = 16$), when applied extracellularly, activated an inward current at −40 mV (Fig. 7*B*). The macroscopic I–V relationship of the conductance was similar to the UVA-induced current, showing both activation and increased noise at higher voltages (see inset in Fig. 7*B*). However, the current magnitude observed with tBOOH might be somewhat underestimated, since tBOOH appears to also be a potent blocker of the current, as witnessed by the large increase in inward current upon discontinuation of its application (Fig. 7*B*). The tBOOH-induced inward current increased by a factor of $5{\cdot}4 \pm 0{\cdot}5$ ($n = 8$) after returning to normal extracellular medium. In addition, tBOOH increased the membrane capacitance by more than 10% during application (Fig. 7*C*). This suggests that tBOOH incorporates itself in the lipid membrane, thus increasing the dielectrical constant. After stopping the application of tBOOH, membrane capacitance decreased again to its initial value or a value up to 10% below its control level prior to tBOOH exposure. Repeated applications of tBOOH after the current had been activated caused reproducible and reversible inhibition of the conductance (Fig. 7*C*). Interestingly, tBOOH was completely ineffective in blocking the current activated by UV light (see second application of tBOOH in Fig. 7*C*).

I_{LiNC} is not activated by oxidized glutathione

Recently, a cationic channel activated by oxidant stress has been described in an endothelial cell line (CPAE) (Koliwad, Elliott & Kunze, 1996*a*; Koliwad *et al.* 1996*b*). To determine

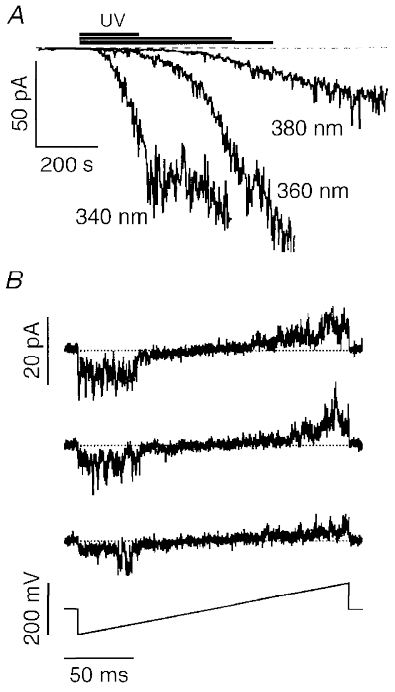

Figure 5. I_{LiNC} is membrane delimited

A, UV light activates a sustained current in outside-out patches from RBL cells that is similar to the whole-cell currents. Three representative experiments illustrate the inward current recorded at a holding potential of −40 mV as a function of wavelength (experimental conditions as in Figs 1*A* and 2*A*). *B*, consecutive high-resolution current traces with 'single channel'-like events evoked by voltage ramps ranging from −100 to +100 mV (data are from the initial activation phase of an experiment in which 340 nm excitation was used).

whether this type of channel could account for the current activated by UV light, we perfused RBL cells with a high cytosolic concentration of oxidized glutathione (GSSG), which has been shown to completely depolarize CPAE cells within 2–5 min (Koliwad *et al.* 1996*a*). In the presence of 4·4 mM GSSG in the standard internal solution, no significant changes in membrane conductance or activation of unspecific currents were observed over a time course of 15 min ($n = 9$, ○, Fig. 8*A*) as compared with control experiments in which internal solutions lacked GSSG ($n = 8$, ●, Fig. 8*A*). Also, there were no significant differences regarding activation of I_{LiNC} after irradiation at 340 nm (Fig. 8*A* and *B*) between both experimental conditions. We should note, though, that in the presence of GSSG – but not in its absence – we often observed the slow development of a small outwardly rectifying current (Fig. 8*B*, left panel, trace 2), resulting in a slight left-shift of the reversal potential and a small positive current at −40 mV compared with control conditions (Fig. 8*B*, right panel, traces 1 and 2). This might be indicative of a potassium conductance, since the pipette solution contained 6·6 mM K_2-EGTA.

In a further set of experiments we asked the question whether or not reduced glutathione (GSH) was able to rescue RBL cells from UV-induced current activation. Perfusing cells with pipette solutions containing 11 mM GSH clearly did not prevent the UV light-induced cation current and in fact, the cells appeared to be even more sensitive to UV light. The slope of activation of I_{LiNC} in the presence of GSH was 44·9 ± 2·5 s ($n = 10$) and hence was significantly faster than paired control experiments where a mean value of 56·3 ± 1·9 s ($n = 7$) was obtained (data not shown).

The above experiments were carried out in the presence of 10 mM Cs^+ in the bath solution to suppress the endogenous inwardly rectifying K^+ current of RBL cells. When extracellular CsCl is removed, extracellular K^+ increased to 20 mM, and K^+-based internal pipette solutions are used, RBL cells show a prominent inwardly rectifying K^+ current. Under these conditions and in the absence of GSSG, the K^+ currents increased slightly with time and reached a steady-state value 1 min after break-in. No inactivation of the K^+ current occurred within 10 min ($n = 12$, ●, Fig. 8*C*). In contrast, an almost complete inhibition of the the inwardly

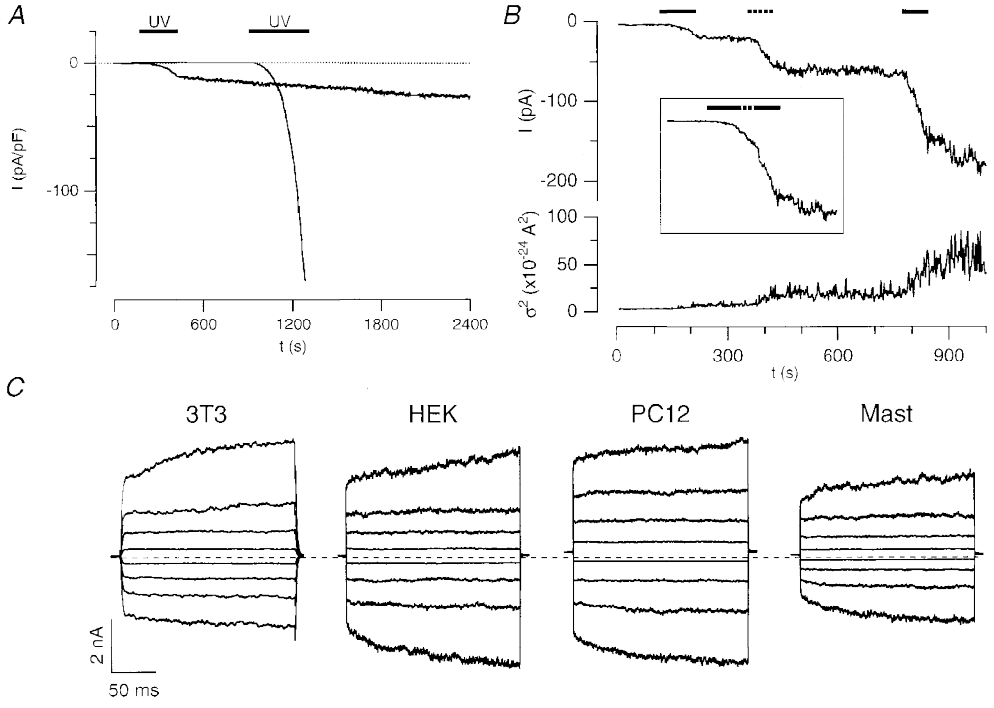

Figure 6. I_{LiNC} is a ubiquitous membrane conductance

A, UV-induced current neither inactivates nor saturates. The panel depicts two typical examples showing inward currents at −40 mV: one cell was illuminated at 340 nm for 3 min shortly after break-in. No inactivation of I_{LiNC} was detected within 30 min of irradiation. The second cell was irradiated 15 min after whole-cell break-in for 6 min (until the end of the experiment) and showed no saturation. *B*, UV-induced membrane conductance is cumulative. An RBL-1 cell was illuminated three times at 340 nm for a total time of 3·5 min (1·5, 1 and 1 min). The inset shows the current without the time between illumination yielding a monophasic activation as seen under continuous illumination. *C*, I_{LiNC} is a ubiquitous phenomenon. A current similar to the one measured in RBL-1 cells could also be activated in 3T3 fibroblasts, human embryonic kidney (HEK), PC12 and mast cells using the same UVA treatment. Records represent currents evoked by voltage pulses in the range ±140 mV at intervals of 40 mV.

rectifying K^+ current occurred within 10 min when the pipette solution was supplemented with 4·4 mM GSSG ($n = 7$, ○, Fig. 8*C*).

To separate the GSSG-induced inhibition of the inwardly rectifying potassium conductance from the UV light-induced non-specific current, the cells kept under control conditions (without GSSG) were irradiated 10 min after break-in at 340 nm (●, Fig. 8*C*, indicated by the bar). This resulted in a slight inactivation of the K^+ currents while simultaneously being sufficient to activate I_{LiNC} (compare traces 3 and 4 in Fig. 8*D*). Thus, GSSG completely inhibited inwardly rectifying K^+ currents without producing any unspecific conductance, while UV illumination caused only a small inhibition of the K^+ current and a strong activation of I_{LiNC}.

DISCUSSION

While many recent investigations have concentrated on delayed UVB and UVC irradiation effects and their role in apoptosis and necrosis (Devary *et al.* 1992; Ziegler *et al.* 1994; Kasid *et al.* 1996), we report here more immediate events due to UVA, the predominant UV species in our atmosphere. Our findings suggest that UV light activates a novel calcium-permeable cationic current. The activation of the UV-induced current occurs in a wavelength- and intensity-dependent manner after treatment of single cells with excess light in the range between 340 and 380 nm. This light-induced cationic current is most probably due to free radical-induced lipid or protein peroxidation, since chemical peroxidants induced a similar current and free radical

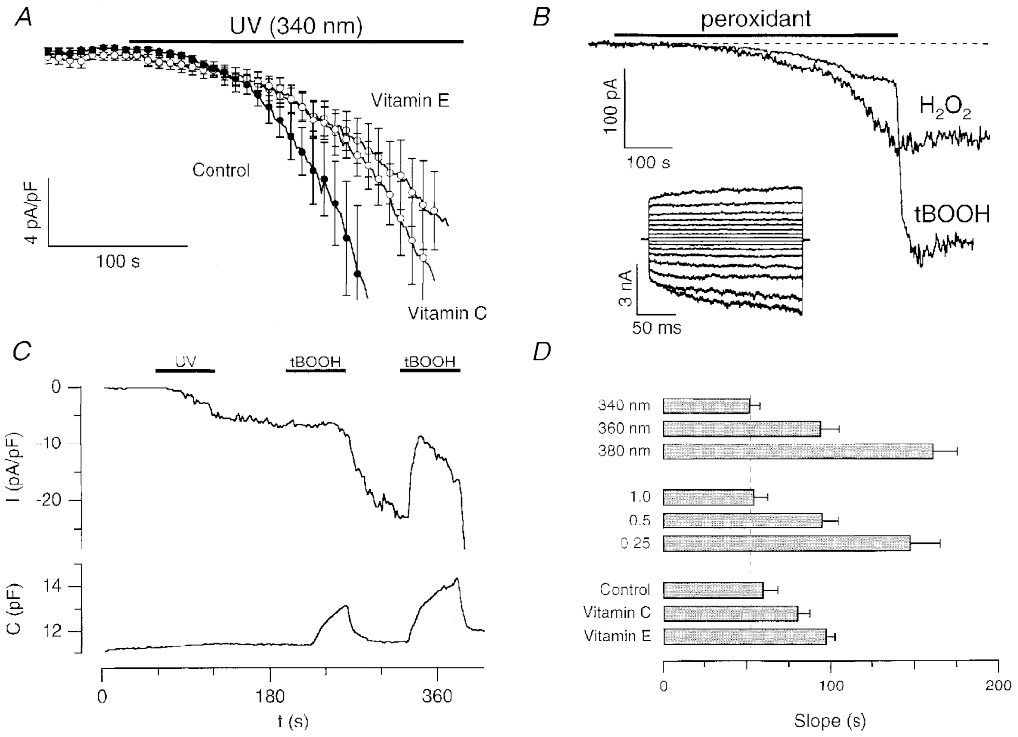

Figure 7. Oxidant stress is involved in activation of I_{LiNC}

A, radical scavengers suppress activation of I_{LiNC}. The panel shows the inward current at −40 mV activated by illumination at 340 nm. A comparison of the UV-induced conductances in control cells and cells that were either preincubated for 2 h with 10 i.u. vitamin E ($n = 8$) or infused by 10 mM vitamin C in the internal solution ($n = 8$) is shown. Mean values ± S.E.M. (control $n = 5$). *B*, oxidant stress activates a current in RBL cells similar to I_{LiNC}. Two representative experiments in which cells were either treated with 3% hydrogen peroxide (H_2O_2, $n = 15$) or 3·5% tert-butylhydroperoxide (tBOOH, $n = 16$) by local application during the time indicated by the bar (10 min) are shown. The inset depicts the *I–V* relationship in the case of the tBOOH-activated current after the end of the application. *C*, tBOOH blocks the tBOOH-activated current. The panel gives a typical example of 5 similar experiments. After activation of I_{LiNC} by irradiation at 340 nm tBOOH was applied twice. The second application blocked a significant portion of the current activated by the first application. However, no inhibition of the UV-induced current by tBOOH could be observed. Note the transient increase in capacitance during application, indicating accumulation of tBOOH in the plasma membrane. *D*, slope of activation of I_{LiNC} *versus* wavelength or light intensity and in the presence of radical chain breaking agents. Cells were either irradiated at different wavelengths of similar intensity (upper bars), at 340 nm with decreasing intensity (middle bars) or at 340 nm of full intensity after treatment with free radical scavengers. Note that the activation of I_{LiNC} after vitamin E treatment is equivalent to a decrease in light intensity of 50% or a shift in excitation wavelength from 340 to 360 nm.

scavengers significantly slowed down the light-induced activation of the current. The similarity of the macroscopic current induced either by UV light or free radicals suggests that UV light is acting through peroxidation and that the cytoplasmic membrane is one – if not the – primary target for both. This conclusion is also supported by the fact that this current can be observed in cell-free membrane patches.

The main question regarding the nature of I_{LiNC} is whether or not it is an endogenous conductance and the observed fluctuations reflect 'real' ion channels. While several features such as voltage dependence, cationic selectivity, and channel-like fluctuations with characteristic noise properties might argue for a classical ion channel, other properties argue against it. (i) I_{LiNC} does not seem to saturate under prolonged continuous illumination. As a result, the membrane resistance decreases continuously with time, ending up at values of less than 20 MΩ and thus making further patch-clamp experiments impossible (Fig. 6*A*). (ii) The current – once activated by UV light or peroxidant treatment – does not inactivate or run down, even over a time period of more than 30 min after the triggering event (Fig. 6*A*). (iii) Activation of the current is cumulative. The final current

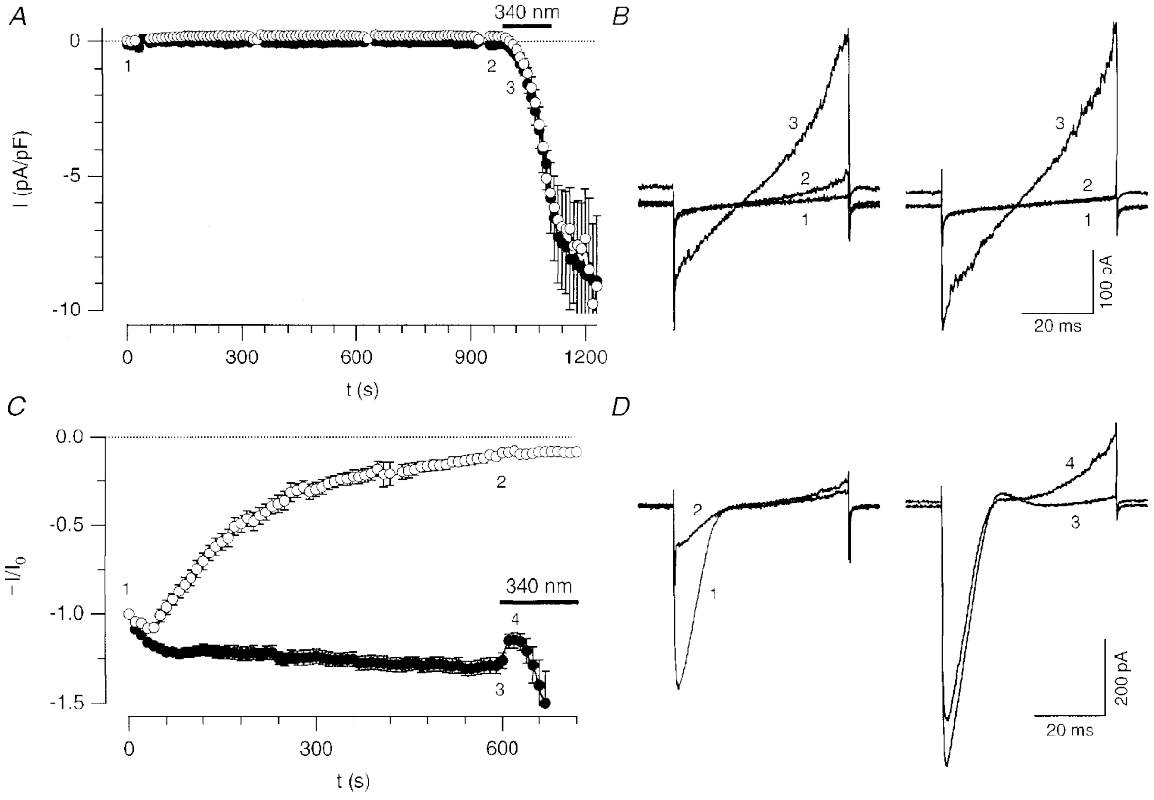

Figure 8. Oxidant stress by oxidized glutathione is not sufficient to activate I_{LiNC}

A, whole-cell current at −40 mV (normalized for cell capacitance) in RBL-2H3 cells. The caesium glutamate-based pipette solution was supplemented with 4·4 mM oxidized glutathione (GSSG, ○, $n = 9$) and potassium currents were blocked by 10 mM CsCl in the bath. GSSG did not activate significant non-selective conductances over a time period of 15 min. This does not differ from paired control experiments without GSSG (control, ●, $n = 8$). The cells were irradiated for 2 min by UV light at 340 nm 15 min after break-in (indicated by the bar), resulting in a similar activation of I_{LiNC} in both cases. Numbers indicate times at which high-resolution current traces as shown in *B* were taken. *B*, high resolution whole-cell *I–V* relationships for 2 typical cells determined by voltage ramps from −100 to +100 mV. The currents were recorded immediately after break-in (1), after 15 min (2, before UV irradiation) and after activation of I_{LiNC} (3) and are not leak subtracted. Right traces correspond to control conditions without GSSG. *C*, GSSG induces inhibition of inwardly rectifying K^+ currents. Whole-cell current at −80 mV (from voltage ramps) normalized to the initial value after break-in is plotted *versus* time. The pipette solution was based on potassium glutamate and CsCl had been omitted from the extracellular medium to obtain inwardly rectifying K^+ currents. Addition of 4·4 mM GSSG to the pipette solution caused an almost complete inhibition of K^+ currents within 10 min (○, $n = 7$), which was not observed in control experiments without GSSG (●, $n = 12$). The latter cells were also UV irradiated (340 nm) 10 min after break-in. Mean values ± S.E.M. are shown. Numbers indicate times at which high-resolution current traces as shown in *D* were taken. *D*, *I–V* relationships from voltage ramps at the time indicated by the labels for two typical cells are shown.

amplitude and the kinetics of its activation are the same regardless of whether the same amount of UV light is applied in a single or several shorter illumination periods (Fig. 6*B*). (iv) The same treatment activated a similar current in cells as different as fibroblasts ($n = 5$), human embryonic kidney cells ($n = 6$), PC12 cells ($n = 11$), mast cells ($n = 5$, Fig. 6*C*) or myoballs ($n = 2$, data not shown). None of these findings alone is a strong argument against an endogenous ion channel, but together they lead us to conclude that I_{LiNC} is a ubiquitous ionic current that is caused by cumulative membrane damage rather than the opening of a native ionic channel. It remains to be determined whether I_{LiNC} constitutes a 'lipidic' pore or a pathway that is produced at the interface of lipids and proteins in biological membranes. Preliminary experiments in pure lipid membranes failed to show UV light-induced conductances, suggesting that either a specific lipid mixture is required or that embedded proteins are necessary to generate such a conductance.

The inability of oxidized glutathione (GSSG) to induce I_{LiNC} sets it apart from a cation channel activated in CPAE cells (Koliwad *et al.* 1996*a*). Nevertheless, GSSG did affect other ionic currents in RBL cells, most notably the inhibition of the inward rectifier. Such GSSG-dependent block of inwardly rectifying K^+ channels, if present in CPAE cells, could in part account for the GSSG-induced depolarization observed in these cells. Since GSSG completely inhibited K^+ currents without producing any unspecific conductance, the GSSG-dependent inhibition may not be due to lipid peroxidation, but may rather be a result of oxidation of thiol groups on free cysteines of the channel itself, as has been proposed as the mechanism of action for several other channels (Koivisto, Siemen & Nedergaard, 1993; Tang & Aizenman, 1993).

While chemical peroxidants also induced a conductance that was in many respects similar to I_{LiNC}, there were also some differences, particularly in the case of tBOOH, which also seemed to inhibit the conductance it activated, but failed to inhibit I_{LiNC}. It thus appears that tBOOH cannot penetrate the pores generated by UV light but can access pores which it produces. The above differences call for a more detailed comparison and it therefore remains to be determined whether or not the membrane conductance induced in both cases is indeed identical at the molecular level. Long-term incubation of endothelial cells with tBOOH has previously been reported to activate a 30 pS cation channel in those cells (Koliwad *et al.* 1996*b*). Those ion channels are clearly different from the ones described in the present study as they are characterized by a larger single channel conductance, the absence of rectification, and different selectivity.

Regardless of the molecular nature of this conductance, as a consequence of its activation by either UV light or free radical stress, cations can enter the cell, leading to membrane depolarization and increases in cytosolic calcium concentration. Thus, the present data can account for several of the primary pathological events observed after free radical stress such as potassium loss (Cardenas *et al.* 1992), cell swelling due to sodium influx (Koliwad *et al.* 1996*b*) and cytoplasmic free calcium increase (Kimura *et al.* 1992). Excessive and/or persistent activation of this conductance might eventually cause cell swelling and ultimately lead to cell death.

Finally, our results allow three interesting conclusions to be made, which may not be unexpected but nevertheless are of great physiological significance. (i) Membrane damage is irreparable in the minutes time range. (ii) As a consequence, this leads to the accumulation of photodamage. (iii) The relationship between the duration of UV irradiation and the activated current is highly non-linear. All three points taken together would imply that a moderate UV exposure may have almost no macroscopic effects; however, an additional irradiation will induce severe cell damage, even at low doses or after a long period of time. This work should also prove to be of particular interest to the numerous investigators using fluorescent probes, specifically in digital imaging and confocal microscopy with its demand on high spatial temporal resolution and therefore rather high doses of excitation light in the UV range. Finally, since the patch-clamp technique turned out to be a suitable tool for studying any peroxidation-induced membrane damage, it should therefore also be a model experimental system to assay potential protective mechanisms in the future.

Beer, J. Z., Olvey, K. M., Miller, S. A., Thomas, D. P. & Godar, D. E. (1993). Non-nuclear damage and cell lysis are induced by UVA, but not UVB or UVC, radiation in three strains of L5178Y cells. *Photochemistry and Photobiology* **58**, 676–681.

Bose, B., Agarwal, S. & Chatterjee, S. N. (1990). Membrane lipid peroxidation by UV-A: mechanism and implications. *Biotechnology and Applied Biochemistry* **12**, 557–561.

Cardenas, A. M., Cortes, M. P., Fernandez, E. & Pena, W. (1992). Lipid peroxidation and loss of potassium from red blood cells produced by phototoxic quinolones. *Toxicology* **72**, 145–151.

Devary, Y., Gottlieb, R. A., Smeal, T. & Karin, M. (1992). The mammalian ultraviolet response is triggered by activation of Src tyrosine kinases. *Cell* **71**, 1081–1091.

Fasolato, C., Hoth, M., Matthews, G. & Penner, R. (1993*a*). Ca^{2+} and Mn^{2+} influx through receptor-mediated activation of nonspecific cation channels in mast cells. *Proceedings of the National Academy of Sciences of the USA* **90**, 3068–3072.

Fasolato, C., Hoth, M. & Penner, R. (1993*b*). A GTP-dependent step in the activation mechanism of capacitative calcium influx. *Journal of Biological Chemistry* **268**, 20737–20740.

Gies, H. P., Roy, C. R., Toomey, S., MacLennan, R. & Watson, M. (1995). Solar UVR exposure of three groups of outdoor workers on the sunshine coast, Queensland. *Photochemistry and Photobiology* **62**, 1015–1021.

Godar, D. E. & Lucas, A. D. (1995). Spectral dependence of UV-induced immediate and delayed apoptosis: the role of membrane and DNA damage. *Photochemistry and Photobiology* **62**, 108–113.

Grynkiewicz, G., Poenie, M. & Tsien, R. (1985). A new generation of Ca^{2+} indicators with greatly improved fluorescence properties. *Journal of Biological Chemistry* **260**, 3440–3450.

Kasid, U., Suy, S., Dent, P., Ray, S., Whiteside, T. L. & Sturgill, T. W. (1996). Activation of Raf by ionizing radiation. *Nature* **382**, 813–816.

Kimura, M., Maeda, K. & Hayashi, S. (1992). Cytosolic calcium increase in coronary endothelial cells after H_2O_2 exposure and the inhibitory effect of U78517F. *British Journal of Pharmacology* **107**, 488–493.

Koivisto, A., Siemen, D. & Nedergaard, J. (1993). Reversible blockade of the calcium-activated nonselective cation channel in brown fat cells by the sulfhydryl reagents mercury and thimerosal. *Pflügers Archiv* **425**, 549–551.

Koliwad, S. K., Elliott, S. J. & Kunze, D. L. (1996*a*). Oxidized glutathione mediates cation channel activation in calf vascular endothelial cells during oxidant stress. *Journal of Physiology* **495**, 37–49.

Koliwad, S. K., Kunze, D. L. & Elliott, S. J. (1996*b*). Oxidant stress activates a non-selective cation channel responsible for membrane depolarization in calf vascular endothelial cells. *Journal of Physiology* **491**, 1–12.

Lavker, R. M., Veres, D. A., Irwin, C. J. & Kaidbey, K. H. (1995). Quantitative assessment of cumulative damage from repetitive exposures to suberythemogenic doses of UVA in human skin. *Photochemistry and Photobiology* **62**, 348–352.

Morliere, P., Moysan, A., Santus, R., Huppe, G., Maziere, J. C. & Dubertret, L. (1991). UVA-induced lipid peroxidation in cultured human fibroblasts. *Biochimica et Biophysica Acta* **1084**, 261–268.

Schnellmann, R. G. (1991). Intracellular calcium chelators and oxidant-induced renal proximal tubule cell death. *Journal of Biochemical Toxicology* **6**, 299–303.

Stark, G. (1991). The effect of ionizing radiation on lipid membranes. *Biochimica et Biophysica Acta* **1071**, 103–122.

Tang, L. H. & Aizenman, E. (1993). The modulation of *N*-methyl-D-aspartate receptors by redox and alkylating reagents in rat cortical neurones *in vitro*. *Journal of Physiology* **465**, 303–323.

Verheij, M., Bose, R., Lin, X. H., Yao, B., Jarvis, W. D., Grant, S., Birrer M. J., Szabo, E., Zon, L. I., Kyriakis, J. M., Haimovitz-Friedman, A., Fuks, Z. & Kolesnick, R. N. (1996). Requirement for ceramide-initiated SAPK/JNK signalling in stress-induced apoptosis. *Nature* **380**, 75–79.

Vile, G. F., Basu-Modak, S., Waltner, C. & Tyrrell, R. M. (1994). Heme oxygenase 1 mediates an adaptive response to oxidative stress in human skin fibroblasts. *Proceedings of the National Academy of Sciences of the USA* **91**, 2607–2610.

Ziegler, A., Jonason, A. S., Leffell, D. J., Simon, J. A., Sharma, H. W., Kimmelman, J., Remington, L., Jacks, T. & Brash, D. E. (1994). Sunburn and p53 in the onset of skin cancer. *Nature* **372**, 773–776.

Acknowledgements

We thank Michael Pilot and Frauke Friedlein for excellent technical assistance and Andrea Fleig, Chris Mathes, Ann Hoffman and Günther Stark for critical comments on the manuscript. We acknowledge support by the following institutions: Deutsche Forschungsgemeinschaft, Sonderforschungsbereich 236, Hermann- und Lilly- Schilling-Stiftung, and the Bundesministerium für Forschung und Technologie.

Corresponding author

R. Penner: Max-Planck-Institute for Biophysical Chemistry, Am Fassberg, 37077 Göttingen, Germany.

Email: rpenner@gwdg.de